Research Square

Preprints are preliminary reports that have not undergone peer review.
They should not be considered conclusive, used to inform clinical practice,
or referenced by the media as validated information.

Posterior cortical gray matter heterogeneity between hyposmia- and RBD-defined prodromal phenotypes in Parkinson's disease: a PPMI voxel-based morphometry study

lingzhuo Chen
Eastern Hepatobiliary Surgery Hospital
Shengqiang Chen
Eastern Hepatobiliary Surgery Hospital
Kejia Hu
Shanghai Jiao Tong University
Hua He
hehua1624@smmu.edu.cn

Eastern Hepatobiliary Surgery Hospital

Research Article

Keywords: Parkinson's disease, prodromal phenotypes, hyposmia, REM sleep behavior disorder, voxel-based morphometry, cuneus

Posted Date: November 1st, 2026

DOI: https://doi.org/10.21203/rs.3.rs-11353584/v1

License: This work is licensed under a Creative Commons Attribution 4.0 International License. Read Full License

Additional Declarations: No competing interests reported.

Abstract

Background

Prodromal Parkinson's disease (PD) includes clinically distinct enrollment phenotypes. We examined whole-brain gray matter volume (GMV) in Parkinson's Progression Markers Initiative (PPMI) participants recruited through hyposmia-only or REM sleep behavior disorder (RBD)-only pathways and assessed the stability of the findings.

Methods

Baseline T1-weighted MRI from 465 hyposmia-only and 149 RBD-only participants (N = 614) was analyzed with CAT12/SPM25 voxel-based morphometry (VBM). Models included age, sex, intracranial volume, and scanner family. Whole-brain clusters were defined at voxel $p < 0.001$ and tested using family-wise error (FWE) correction. We examined scanner-restricted samples, 123 sex/scanner-matched pairs, and 10,000-sign-flip permutation analysis of linear models (PALM). Bilateral cuneus/calcarine estimates and clinical assessments were exploratory.

Results

Whole-brain analysis identified a posterior phenotype effect (F cluster: k = 4,499; pFWE = 4.15×10^{-7}), with higher GMV in hyposmia-only participants. In 123 matched pairs, a posterior H > RBD T cluster survived correction (pFWE = 0.0266), whereas the F contrast did not. PALM also identified a posterior effect (two-sided threshold-free cluster enhancement [TFCE] FWE p = 0.0027; voxelwise FWE p = 0.0277). Adjusted bilateral cuneus differences were + 0.211 mL (95% CI 0.095–0.327) in the full cohort and + 0.187 mL (0.041–0.333) after matching. MRI-proximal RBD screening questionnaire scores showed no significant association with regional GMV.

Conclusions

Posterior cortical GMV differed between these enrollment-defined prodromal phenotypes. The anatomical finding was supported by nonparametric inference, although the matched F test and strictest scanner restriction were nonsignificant. Longitudinal studies are needed to establish its clinical relevance.

1. Introduction

Prodromal Parkinson's disease (PD) is clinically heterogeneous. Olfactory dysfunction, sleep disturbances, and other nonmotor abnormalities can precede motor diagnosis by years. The Movement Disorder Society (MDS) research criteria use combinations of risk factors and prodromal markers to estimate the probability of prodromal PD (Berg et al. 2015; Berg et al. 2021; Chopra et al. 2024; Heinzel et al. 2019; Schapira et al. 2017; Wullner et al. 2023). Imaging studies that pool people recruited through different markers may miss

regional differences related to those entry phenotypes. The Parkinson's Progression Markers Initiative (PPMI), which includes several prodromal recruitment pathways alongside early PD, offers an opportunity to examine this question using standardized clinical and MRI assessments (Marek et al. 2011; Marek et al. 2018; Siderowf et al. 2026).

Rapid eye movement sleep behavior disorder (RBD) and hyposmia are prominent prodromal markers with partly different clinical associations. Isolated RBD carries a high risk of subsequent synucleinopathy. Neuroimaging studies have reported changes in brainstem, limbic, temporal, posterior, and distributed network regions in RBD-related populations (Campabadal et al. 2021; Di Folco et al. 2024; Garcia-Gomar et al. 2022; Grimaldi et al. 2023; Guo et al. 2018; Oltra et al. 2022; Postuma et al. 2019; Valli et al. 2022; Wang et al. 2024; Yang et al. 2020). Olfactory impairment has been associated with alterations across olfactory–limbic and prefrontal circuits, including the amygdala, entorhinal and parahippocampal regions, insula, and orbitofrontal cortex (Brosse et al. 2024; Fullard et al. 2017; Lyu et al. 2021; Orso et al. 2024; Saqib et al. 2025). Although the markers may coexist, their differing clinical and imaging associations suggest that enrollment-defined groups merit direct comparison (Berg et al. 2021; Horsager and Borghammer 2024; Lyu et al. 2021; Orso et al. 2024).

Voxel-based morphometry (VBM) provides a whole-brain measure of structural variation from T1-weighted MRI (Ashburner and Friston 2000; Gaser et al. 2024). Findings in PD and RBD-related samples vary with clinical phenotype, disease stage, scanner platform, and analytical approach (Campabadal et al. 2021; Grimaldi et al. 2023; Oltra et al. 2022; Valli et al. 2022; Wang et al. 2024; Yang et al. 2020). In a recent PPMI analysis, Zhao et al. (2026) used age- and sex-matched groups and FreeSurfer/ScLimbic morphometry to examine predefined olfactory–limbic and Papez-related regions, together with structural covariance. Their findings focused on limbic systems. Whole-brain VBM asks a complementary question: where are the largest adjusted structural differences between the recruitment phenotypes, including outside those predefined regions? We also evaluated whether the resulting localization was sensitive to scanner composition or statistical inference, both important considerations in multicenter MRI studies (Fortin et al. 2018; Orlhac et al. 2022).

We compared GMV between mutually exclusive hyposmia-only and RBD-only participants enrolled in PPMI from 2020 onward. The primary analysis used an unrestricted whole-brain, direction-independent phenotype contrast, adjusted for age, sex, total intracranial volume (TIV), and scanner family. We then assessed scanner and tissue-mask restrictions. Secondary comparisons with manifest PD provided disease context. Following the whole-brain finding, we examined exact sex/scanner matching, nonparametric PALM inference, atlas-defined posterior regional effects, and clinical measures. These analyses assessed the stability and interpretation of the original finding.

2. Materials and Methods

2.1. Data source, cohort construction, and phenotype definition

Data came from PPMI, a multicenter observational study with standardized clinical, biomarker, and imaging assessments (Marek et al. 2011; Marek et al. 2018). We selected T1-weighted scans from the official baseline MRI visit. Of 1,236 candidate examinations, 1,230 could be linked to the clinical analysis table. Image quality control excluded 54 unique scans, leaving a QC-passed parent cohort of 1,176 participants. The principal comparison concerned prodromal enrollment phenotypes, with manifest PD included for secondary disease-context analyses. Figure 1 shows the cohort flow and analytical framework.

Phenotype analyses included participants enrolled on or after 1 January 2020, consistent with the contemporary PPMI prodromal recruitment structure (Siderowf et al. 2026). Groups were assigned using PPMI participant-status variables. Hyposmia-only required ENRLHPSM = 1, ENRLRBD = 0, ENRLLRRK2 = 0, and ENRLGBA = 0. RBD-only required ENRLRBD = 1, ENRLHPSM = 0, ENRLLRRK2 = 0, and ENRLGBA = 0. These criteria excluded overlapping RBD/hyposmia enrollment and positive LRRK2/GBA mutation-at-enrollment flags. The resulting cohort comprised 465 hyposmia-only and 149 RBD-only participants (N = 614), all scanned at 3 T. Group labels throughout refer to these PPMI enrollment categories.

The PPMI protocol was approved by the institutional review board or independent ethics committee at each participating site and was conducted in accordance with the Declaration of Helsinki and applicable regulatory requirements. All participants provided written informed consent before study procedures. The present analysis used de-identified previously collected data and involved no new participant contact.

2.2. Inclusion and exclusion criteria

Imaging analyses required an official PPMI baseline T1-weighted scan, a matching clinical record, acceptable MRI quality control, and complete age, sex, TIV, group, and scanner-family data. The primary phenotype comparison further required enrollment from 1 January 2020 onward and membership in one of the two mutually exclusive groups described above. All 614 participants in that comparison had 3-T MRI.

The RBD-only category was identified from enrollment-status data. Participant-level polysomnography was not independently reassessed, so RBD status in this report denotes the PPMI recruitment phenotype.

Manifest PD participants were included as a secondary disease-context group. We did not include healthy controls in the principal phenotype comparison, which was designed to compare the two prodromal recruitment groups directly.

2.3. Clinical and neuropsychological assessments

PPMI enrollment variables (ENRLHPSM and ENRLRBD) determined phenotype membership. Questionnaires and cognitive or motor scales were analyzed as clinical descriptors. MDS-UPDRS Part I patient questionnaire and Part II totals were available for the full primary cohort. For MDS-UPDRS Part III and Montreal Cognitive Assessment (MoCA), records within +/-90 days of MRI were selected when available (Goetz et al. 2008; Nasreddine et al. 2005). Together, these measures characterized nonmotor symptoms, daily motor function, motor examination findings, and cognition.

Clinical measures also included the University of Pennsylvania Smell Identification Test (UPSIT; Doty et al. 1984) and the REM Sleep Behavior Disorder Screening Questionnaire (RBDSQ; Stiasny-Kolster et al. 2007). We distinguished screening-visit (SC) UPSIT and baseline-visit (BL) RBDSQ records from subsequent assessments. Source information dates (INFODT) were available by month and year, while MRI acquisition dates were recorded by day. An assessment was considered certainly within ± 90 days of MRI only if the entire possible assessment month fell inside that window. The questionnaire results were used to describe participants recruited through the two enrollment pathways.

2.4. MRI acquisition, preprocessing, and quality control

Structural T1-weighted MRI was acquired across participating PPMI sites using standardized site-specific 3-D T1-weighted protocols, including MPRAGE, FSPGR/BRAVO, and platform-specific equivalents. Acquisition parameters varied across sites and scanner models. All scans in the primary phenotype cohort were 3 T; scanner family was modeled explicitly to account for remaining platform heterogeneity.

Images were processed using CAT12.9 (revision 2577) within SPM25 (version 25.01.02). T1-weighted images were segmented into tissue classes, spatially normalized to standard space, and modulated to preserve local GMV. Modulated normalized gray matter maps were smoothed with an 8-mm full-width at half-maximum Gaussian kernel for whole-brain VBM (Ashburner and Friston 2000; Gaser et al. 2024).

Quality control combined the CAT12 image quality rating with a multimetric whole-brain tissue-volume plausibility procedure. Scans with a CAT12 image quality rating below 80% or unavailable quality information were classified as failing the CAT12 criterion. For volume-based QC, an automated screen evaluated TIV, gray matter (GM), white matter (WM), cerebrospinal fluid (CSF), and the derived ratios GM/TIV, WM/TIV, CSF/TIV, and GM/WM. Candidate outliers were flagged using an absolute z score > 3, a median-absolute-deviation-based modified z score > 3.5, or values outside the 3 x interquartile-range bounds; sex-stratified absolute z scores > 3 were additionally applied to the four raw tissue-volume measures. Flagged cases were reviewed, resulting in 46 tissue-volume QC exclusions. Seventeen scans failed the CAT12 quality criterion and 9 met both criteria, yielding 54 unique exclusions. Primary VBM used implicit masking with an absolute gray matter threshold of 0.05. No proportional scaling or global normalization of GMV was applied.

2.5. VBM analysis design

2.5.1. Primary phenotype VBM

The primary whole-brain model compared Hyposmia-only (n = 465) and RBD-only (n = 149) participants using independent groups with unequal variance. Age, sex, TIV, and scanner family were included as nuisance covariates. Siemens PRISMA was the reference scanner category, with indicator variables for GE ARCHITECT, GE MR750, Other, Siemens SKYRA, Siemens VERIO, and Siemens VIDA. The design contained 614 observations, 11 estimable columns, and was full rank.

The primary inferential test was a one-degree-of-freedom, direction-independent phenotype F contrast. Directional T contrasts (Hyposmia-only > RBD-only and RBD-only > Hyposmia-only) were used to describe the direction and spatial extent of significant effects. Statistical maps were thresholded at voxel $P < 0.001$

uncorrected, followed by cluster-level FWE correction at P_FWE < 0.05, without an additional extent threshold.

2.5.2. Tissue mask and scanner-composition restrictions

Four sensitivity analyses were defined to test whether the primary phenotype effect depended on tissue masking or scanner composition. First, the primary N = 614 model was repeated with a stricter absolute gray matter mask of 0.10. Second, a scanner common-support cohort retained scanner families only when both phenotypes contained at least five participants, yielding 292 Hyposmia-only and 135 RBD-only participants (N = 427; GE ARCHITECT, GE MR750, Siemens PRISMA, and Siemens SKYRA). Third, the analysis was restricted to Siemens 3-T PRISMA and SKYRA scanners (262 Hyposmia-only, 98 RBD-only; N = 360), with scanner platform retained as a covariate. Fourth, the strictest analysis used Siemens PRISMA only (208 Hyposmia-only, 79 RBD-only; N = 287), eliminating the scanner-family covariate. All other preprocessing and inferential settings were unchanged.

2.5.3. Post hoc sex- and scanner-family-matched VBM

We addressed the marked sex and scanner imbalance through 1:1 matching of RBD-only to hyposmia-only participants without replacement. Matches were exact for sex and scanner family, with the total absolute age difference minimized among the maximum feasible set. This yielded 123 pairs (N = 246; 26 RBD-only participants unmatched). Paired VBM used the original smoothed modulated GM images and mask 0.05, with fixed effects for each pair and terms for phenotype, age, and TIV. Sex and scanner family were constant within each pair and were therefore omitted as separate regressors. We evaluated a direction-independent F contrast and directional T contrasts. The design had 246 observations and 127 columns, rank 126, and 120 residual degrees of freedom. The phenotype contrast was checked for estimability despite the redundant design column (Supplementary Table S4).

2.5.4. Nonparametric whole-brain inference

We applied permutation analysis of linear models (PALM) to the original N = 614 dataset using the same SPM scan order, design, phenotype contrast, and mask (Winkler et al. 2014). The model retained age, sex, TIV, and scanner family. We used 10,000 independent residual sign-flips, Freedman–Lane nuisance adjustment, and phenotype-specific variance groups for two-sided whole-brain FWE inference. Threshold-free cluster enhancement (TFCE; Smith and Nichols 2009) was the principal endpoint; voxelwise maximum-statistic and cluster-extent FWE were secondary. We checked the sign of each significant voxel against the original SPM hyposmia-minus-RBD contrast because two-sided corrected P maps contain no direction information. This form of sign-flipping assumes approximately independent and symmetric residual errors.

2.5.5. Secondary disease-context analyses with manifest PD

Secondary analyses placed the phenotype findings in the context of manifest PD. The full disease-context cohort included post-2020 Hyposmia-only (n = 465), RBD-only (n = 149), and PD (n = 316) participants after restricting all three groups to 3 T (N = 930). A three-group model included age, sex, TIV, and scanner family, with independent groups and unequal variance. An omnibus group F test was followed by pairwise direction-independent F contrasts. Because the primary H-RBD hypothesis had already been tested in the dedicated two-group analysis, the disease-context inferential family comprised two comparisons: Hyposmia-only

versus PD and RBD-only versus PD. These were evaluated using a Bonferroni-adjusted alpha of 0.025; corresponding directional T contrasts established effect direction.

Scanner robustness was assessed in two additional disease-context cohorts. A three-group common-support analysis retained scanner families with at least five participants in each group (292 Hyposmia-only, 135 RBD-only, 256 PD; N = 683). A further Siemens 3-T PRISMA/SKYRA restriction included 262 Hyposmia-only, 98 RBD-only, and 224 PD participants (N = 584). The same disease-context contrast family and inferential thresholds were retained.

2.5.6. Post hoc atlas-defined regional GMV and imaging–clinical associations

Bilateral cuneus and calcarine masks were constructed from the SPM Neuromorphometrics atlas (cuneus labels 114/115; calcarine 108/109), resampled to the GM image grid by nearest-neighbor interpolation. For each participant, modulated normalized smoothed GM intensities were integrated over each atlas mask and multiplied by the voxel volume. Values are nominal milliliter-equivalent atlas-integrated modulated GM measures, not native-space anatomical tissue volumes. Full-cohort (N = 614) ROI group differences were estimated by linear models adjusted for age, sex, TIV, and scanner family; HC3 heteroskedasticity-consistent standard errors provided approximate 95% confidence intervals (MacKinnon and White 1985). For the frozen 123 pairs, per-pair hyposmia-minus-RBD ROI differences were regressed on within-pair age and TIV differences, with the intercept representing the adjusted contrast at zero covariate differences. The two ROIs were tested as a separate post hoc exploratory family, with Benjamini–Hochberg FDR adjustment (Benjamini and Hochberg 1995).

For exploratory brain–symptom analyses, we used RBDSQ-BL records classified as certainly within ± 90 days of MRI (N = 606: 462 hyposmia-only, 144 RBD-only). Models included phenotype, age, sex, TIV, and scanner family and estimated overall RBDSQ slopes and phenotype-by-RBDSQ interactions. Within-group analyses and analyses of all dated BL records assessed sensitivity to the sample definition. FDR correction was applied separately to the two ROIs within each analysis type. UPSIT was excluded as an MRI-proximal imaging predictor because the screening assessment often preceded MRI substantially, especially among hyposmia-only participants. Anatomical ROI selection followed the whole-brain finding, so the regional analyses were considered exploratory (Kriegeskorte et al. 2009).

2.6. Statistical analysis and multiple-comparison control

The primary hypothesis was tested with a one-degree-of-freedom F contrast, allowing an effect in either direction. Signed T contrasts characterized the two directions. Although the F and T contrasts refer to the same underlying group coefficient, the F test and one-sided directional T test use different voxel-forming thresholds at nominal $P < 0.001$. Consequently, their clusters and corrected cluster P values can differ, as seen in the matched analysis. Parametric VBM used voxel $p < 0.001$ uncorrected, followed by whole-brain cluster-level FWE $p < 0.05$, with no minimum extent requirement. The two secondary comparisons with PD formed a separate family with Bonferroni correction (raw cluster-FWE $p < 0.025$, corresponding to adjusted $p < 0.05$). Scanner/mask restrictions and matched VBM were sensitivity analyses. The two-sided PALM

analysis used TFCE-FWE $p < 0.05$ as its main endpoint, with voxelwise maximum-statistic and cluster-extent inference reported secondarily (Smith and Nichols 2009; Winkler et al. 2014).

Continuous MDS-UPDRS and MoCA scores were summarized by median and interquartile range and compared with two-sided Mann–Whitney tests; rank-biserial effect sizes and Benjamini–Hochberg FDR values were calculated across those four broad clinical outcomes. Age and TIV were described as mean ± SD and assessed descriptively by Welch tests, and sex/scanner composition by chi-square statistics and Cramér's V. Visit-filtered UPSIT and RBDSQ scores were also compared using age-, sex-, and scanner-adjusted linear models with HC3 robust standard errors, reporting adjusted between-group differences and 95% confidence intervals; matched questionnaire comparisons used available complete pairs and within-pair age-difference adjustment. Within-phenotype UPSIT–RBDSQ partial rank correlations were exploratory. Questionnaire analyses were not included as additional covariates in the main imaging tests because these measures are related to enrollment pathways. Separate prespecified test families and post hoc exploratory families are distinguished explicitly in the Results and Supplementary Information. Statistical analyses used MATLAB R2024b and image processing used CAT12.9/SPM25.

3. Results

3.1. Primary phenotype cohort and clinical profile

The primary cohort included 465 Hyposmia-only and 149 RBD-only participants (N = 614), all scanned at 3 T. Mean age was similar between groups (67.95 +/- 5.36 versus 68.08 +/- 5.83 years; P = 0.812; Hedges g=-0.02). The RBD-only group had a higher proportion of men (76.5% versus 39.4%; chi-square P < 0.001; Cramer's V = 0.319) and higher mean TIV (1495.8 +/- 144.1 versus 1450.7 +/- 135.9 mL; P = 0.0009; g=-0.33 for Hyposmia-minus-RBD). Scanner distribution also differed between phenotypes (chi-square = 117.16, df = 6, P = 6.42x10^-23; Cramer's V = 0.437), motivating the planned scanner sensitivity analyses. Demographic and clinical characteristics are summarized in Table 1.

Table 1
Demographic and clinical characteristics of the primary enrollment-defined phenotype cohort.

Characteristic	Hyposmia-only (n = 465)	RBD-only (n = 149)	P	Effect / FDR
Age, years	67.95 +/- 5.36	68.08 +/- 5.83	0.812	Hedges g=-0.02
Male sex, n (%)	183 (39.4)	114 (76.5)	< 0.001	Cramer's V = 0.319
TIV, mL	1450.7 +/- 135.9	1495.8 +/- 144.1	0.0009	Hedges g=-0.33
MDS-UPDRS Part I patient	5 [2–7] (n = 465)	5 [3–8] (n = 149)	0.049	q = 0.066; r_rb=-0.106
MDS-UPDRS Part II	1 [0–3] (n = 465)	1 [0–4] (n = 149)	0.032	q = 0.064; r_rb=-0.111
MDS-UPDRS Part III (+/-90 d)	3 [1–5] (n = 448)	4 [2–6] (n = 141)	0.024	q = 0.064; r_rb=-0.125
MoCA total (+/-90 d)	27 [25–28] (n = 460)	27 [25–28] (n = 145)	0.404	q = 0.404; r_rb=-0.046
UPSIT (SC screening)	22.30 ± 7.39 (n = 465)	24.47 ± 8.39 (n = 146)	2.32×10^{-6} †	Adj. H − RBD − 4.00; q = 2.32×10^{-6}
RBDSQ (BL baseline)	4.54 ± 3.73 (n = 465)	9.76 ± 2.47 (n = 148)	6.43×10^{-36} †	Adj. H − RBD − 4.58; q = 1.29×10^{-35}

Age and TIV are mean ± SD; the four original MDS-UPDRS/MoCA scales are median [IQR], with two-sided Mann–Whitney nominal P, rank-biserial effect rrb, and BH-FDR q across those four tests. †UPSIT/RBDSQ are mean ± SD for specified visits; P values are from age-, sex-, and scanner-adjusted HC3 linear models, with a separate two-scale FDR family. Their timing relative to MRI differs markedly; see Supplementary Table S5. Sex and age/TIV tests are descriptive. H=Hyposmia-only; RBD = RBD-only.

Across the four broad clinical measures, nominal MDS-UPDRS Part I–III differences favored greater symptom burden in RBD-only participants, although none survived FDR correction; median MoCA was the same in both groups (Table 1). UPSIT scores at screening were lower in hyposmia-only participants (adjusted H − RBD difference − 4.00, 95% CI − 5.64 to − 2.35; $q = 2.32\times10^{-6}$), whereas baseline RBDSQ scores were higher in RBD-only participants (adjusted H − RBD difference − 4.58, 95% CI − 5.26 to − 3.91; $q = 1.29\times10^{-35}$). Unadjusted H − RBD mean differences were − 2.17 for UPSIT and − 5.22 for RBDSQ. Adjustment altered the estimates, particularly for UPSIT, but the contributions of individual covariates were not separately decomposed. Before visit-specific filtering, 612/614 participants had a UPSIT score and 614/614 had an RBDSQ score. Restriction to screening UPSIT (SC) retained 611 participants (465 hyposmia-only, 146 RBD-only); restriction to baseline RBDSQ (BL) retained 613 (465 and 148, respectively). Only 19/465 hyposmia-only UPSIT screening records were certainly within MRI ± 90 days, compared with 462/465 hyposmia-only and 144/148 RBD-only BL RBDSQ records (Supplementary Table S5).

3.2. Primary whole-brain phenotype difference

The primary direction-independent phenotype F test identified one large posterior cortical cluster (k = 4,499, cluster P_FWE = 4.15x10^-7; peak F = 25.81 at MNI [0, -91.5, 22.5]). The corresponding directional analysis showed greater posterior GMV in Hyposmia-only than RBD-only participants (k = 5,947, cluster P_FWE = 1.33x10^-7; peak T = 5.08 at the same coordinate), whereas no cluster survived correction for RBD-only > Hyposmia-only. The cluster was centered in posterior occipital/cuneus territory and extended through adjacent visual cortex (Fig. 2A,B).

3.3. Mask and scanner-composition robustness

The posterior F cluster survived a stricter absolute GM mask of 0.10 (N = 614; k = 3,830, pFWE = 3.46×10^{-6}), restriction to scanner families represented in both phenotypes (N = 427; k = 3,127, pFWE = 1.97×10^{-5}), and the Siemens PRISMA/SKYRA subset (N = 360; k = 1,547, pFWE = 0.00269). Peaks remained in comparable posterior territory (Table 2; Supplementary Fig. S1, Online Resource 1). In the PRISMA-only subset (N = 287), a posterior cluster was still evident at the voxel-forming threshold but did not reach cluster-FWE significance (F: k = 381, pFWE = 0.273; directional H > RBD: k = 564, pFWE = 0.156). The smaller cohort and its selected participant/site composition cannot be separated as explanations for this attenuation.

Table 2
Primary Hyposmia-only versus RBD-only whole-brain VBM and robustness analyses.

Analysis	Restriction	N	k	Cluster P_FWE	Peak statistic; MNI	Direction
Primary	All post-2020 phenotype scans; mask 0.05	614	4,499	4.15x10^-7	F = 25.81; [0, -91.5, 22.5]	H > RBD; T = 5.08
Mask sensitivity	Same cohort; mask 0.10	614	3,830	3.46x10^-6	F = 25.83; [0, -91.5, 22.5]	H > RBD; T = 5.08
Common support	Scanner families > = 5/group	427	3,127	1.97x10^-5	F = 22.30; [0, -91.5, 24]	H > RBD; T = 4.72
Siemens 3 T	PRISMA + SKYRA	360	1,547	0.00269	F = 20.08; [-1.5, -87, 27]	H > RBD; T = 4.48
Single platform	PRISMA only	287	381*	0.273*	F = 16.06; [0, -88.5, 25.5]	No corrected F cluster; concordant H > RBD peak

*The PRISMA-only values are the largest spatially concordant posterior clusters at voxel P < 0.001; they did not survive cluster-level FWE correction. Primary inference was the direction-independent phenotype F test. Directional T maps established effect direction.

3.4. Sex/scanner matching and nonparametric whole-brain inference

Exact sex/scanner-family matching yielded 123 H–RBD pairs (N = 246). Mean age was 68.80 years in hyposmia-only and 68.63 years in RBD-only participants; the mean absolute within-pair age difference was

0.626 years. The paired F contrast was not cluster-FWE significant (minimum pFWE = 0.3795). A directional H > RBD T cluster was detected posteriorly (k = 996, pFWE = 0.0266; peak T = 4.18 at MNI [− 28.5, − 103.5, 12]), with no corrected cluster for the reverse contrast. The matched peak was more leftward and posterior than the primary peak. We report the F and T results separately because their cluster-forming thresholds and inference differ (Fig. 2C; Supplementary Table S4).

Two-sided PALM inference using 10,000 sign-flips in the original N = 614 cohort identified posterior corrected significance under the primary TFCE-FWE approach (minimum pFWE = 0.0027; 8,967 significant voxels). Voxelwise maximum-statistic FWE also detected 50 significant voxels (minimum pFWE = 0.0277; minimum-P coordinate [0, − 91.5, 24]), and cluster-extent FWE was significant (minimum pFWE = 0.0021; 3,562 significant voxels). In a post hoc direction audit against the original signed SPM contrast, all PALM-significant voxels had H > RBD signs. Of the 8,967 TFCE-significant voxels, 6,382 (71.2%) also exceeded the original SPM positive T threshold at voxel p < 0.001 uncorrected; this is not overlap between two FWE-corrected masks. The PALM voxelwise peak was 1.5 mm from the primary SPM peak, supporting localization consistency (Fig. 2D; Supplementary Tables S8–S9).

3.5. Disease-context analyses

In the full post-2020 all-3-T disease-context cohort (N = 930), the omnibus group test showed a large posterior effect (k = 4,511, P_FWE = 6.42x10^-8; peak F = 14.36 at [1.5, -88.5, 18]). The H-RBD contrast also reproduced the posterior phenotype difference (F: k = 2,923, P_FWE = 2.26x10^-5; peak F = 22.42), providing an internal consistency check within the three-group model (Supplementary Table S2, Panel C; Online Resource 1).

The principal disease-context finding was a robust posterior difference between Hyposmia-only and PD. In the full all-3-T cohort, Hyposmia-only versus PD yielded k = 3,907 (P_FWE = 1.47x10^-6; two-comparison adjusted P = 2.94x10^-6; peak F = 25.64 at [1.5, -79.5, 10.5]), with the directional map showing Hyposmia-only > PD (k = 4,887, P_FWE = 9.14x10^-7; peak T = 5.06; Supplementary Table S2, Panel C). This effect remained significant in the three-group common-support cohort (N = 683; k = 3,283, P_FWE = 1.11x10^-5; adjusted P = 2.22x10^-5; peak F = 21.18 at [0, -90, 12]) and after Siemens PRISMA/SKYRA restriction (N = 584; k = 1,954, P_FWE = 0.000566; adjusted P = 0.00113; peak F = 17.83 at [0, -87, 12]).

The RBD-only versus PD comparison was less consistent. No corrected cluster was found in the full N = 930 cohort. In the common-support sample (N = 683), the F comparison detected a left striatal cluster (k = 1,344, P_FWE = 0.00471; adjusted P = 0.00942; peak F = 20.44 at [-24, -7.5, 0]), with a directional PD > RBD T cluster (k = 1,795, P_FWE = 0.00245; Supplementary Table S2, Panel C). The corresponding Siemens-only F contrast did not survive correction (N = 584; minimum cluster P_FWE = 0.088). This platform-dependent result was retained as a secondary observation (Table 3; Supplementary Fig. S2, Online Resource 1).

Table 3
Disease-context phenotype-versus-PD analyses across acquisition restrictions.

Cohort	Comparison	H/RBD/PD (N)	k	Cluster P_FWE	Family-adjusted P	Peak statistic; MNI	Direction
Full all-3-T	H vs PD	465/149/316 (930)	3,907	1.47x10^-6	2.94x10^-6	F = 25.64; [1.5, -79.5, 10.5]	H > PD
Full all-3-T	RBD vs PD	465/149/316 (930)	368*	0.280*	0.560*	F = 17.04; [-24, -7.5, 0]	No corrected difference
Common support	H vs PD	292/135/256 (683)	3,283	1.11x10^-5	2.22x10^-5	F = 21.18; [0, -90, 12]	H > PD
Common support	RBD vs PD	292/135/256 (683)	1,344	0.00471	0.00942	F = 20.44; [-24, -7.5, 0]	PD > RBD
Siemens 3 T	H vs PD	262/98/224 (584)	1,954	0.000566	0.00113	F = 17.83; [0, -87, 12]	H > PD
Siemens 3 T	RBD vs PD	262/98/224 (584)	626*	0.0881*	0.176*	F = 21.31; [15, 6, 55.5]	No corrected difference

H=Hyposmia-only; RBD = RBD-only; PD=manifest Parkinson's disease. Family-adjusted P values use Bonferroni correction across the two disease-context F tests (H vs PD and RBD vs PD). *Largest cluster shown when the pairwise F map did not survive cluster-level FWE correction.

3.6. Exploratory posterior ROI effect sizes and RBDSQ associations

Bilateral atlas-defined cuneus and calcarine measures showed positive adjusted H − RBD differences in the primary cohort: cuneus + 0.211 mL (95% CI + 0.095 to + 0.327) and calcarine + 0.165 mL (+ 0.068 to + 0.262), both FDR q < 0.001. In the matched sample, the cuneus contrast remained significant (+ 0.187 mL, + 0.041 to + 0.333; q = 0.0253), while the calcarine interval included zero (+ 0.110 mL, − 0.022 to + 0.242; q = 0.101). These estimates quantify regions selected after the whole-brain analysis (Fig. 3; Table 4; Supplementary Table S6).

MRI-proximal RBDSQ-BL scores were available for 606 participants. Neither bilateral ROI showed an FDR-significant adjusted association (cuneus slope − 0.00338 mL/point, q = 0.586; calcarine − 0.00743, q =

0.353). Phenotype-by-RBDSQ interactions and within-group slopes were also nonsignificant (Supplementary Table S7). UPSIT–RBDSQ partial rank correlations within the two enrollment groups were weak (hyposmia-only ρ=−0.120, q = 0.0205; RBD-only ρ=−0.108, q = 0.209; Supplementary Table S5); these results do not demonstrate a difference between the group-specific correlations.

Table 4
Exploratory bilateral posterior ROI contrasts in original and matched cohorts and MRI-proximal RBDSQ associations.

Bilateral ROI	Original cohort (N = 614) H − RBD Δ (95% CI); q	Matched (123 pairs) H − RBD Δ (95% CI); q	RBDSQ (N = 606) β mL/point (95% CI); q
Cuneus	+ 0.211 (+ 0.095 to + 0.327) q = 0.00074	+ 0.187 (+ 0.041 to + 0.333) q = 0.0253	−0.00338 (− 0.01558 to + 0.00882) q = 0.586
Calcarine cortex	+ 0.165 (+ 0.068 to + 0.262) q = 0.00091	+ 0.110 (− 0.022 to + 0.242) q = 0.101	−0.00743 (− 0.01823 to + 0.00336) q = 0.353

H − RBD=Hyposmia-only minus RBD-only. ROI values are atlas-integrated smoothed modulated GM signal (nominal mL), not native-space tissue volume. HC3-robust CIs and two-ROI BH-FDR are exploratory; RBDSQ measures were MRI-proximal (N = 606). See Tables S6–S7.

4. Discussion

4.1. Posterior morphology differentiates enrollment phenotypes

The strongest morphological difference between enrollment-defined hyposmia-only and RBD-only participants involved posterior cortex. The primary direction-independent VBM analysis localized a cluster to cuneus/calcarine and adjacent visual areas, with higher GMV in the hyposmia-only group. PALM showed whole-brain corrected significance under both TFCE and voxelwise maximum-statistic inference. The latter's peak was 1.5 mm from the parametric peak, and every PALM-significant voxel had a positive H − RBD sign in the original SPM contrast. This agreement in location and direction across inferential approaches reduces concern that the posterior finding depends solely on parametric cluster-extent correction (Smith and Nichols 2009; Winkler et al. 2014).

Posterior visual regions have also been implicated in structural and multimodal studies of RBD-related conditions (Campabadal et al. 2021; Grimaldi et al. 2023; Oltra et al. 2022; Yang et al. 2020). Our result describes relative gray-matter morphology between two recruitment groups. As the comparison lacks a healthy control group and longitudinal imaging, it cannot establish atrophy in either group or specify a pathological process.

The cuneus effect remained positive after matching, with a confidence interval that excluded zero. The matched calcarine estimate was also positive, but less precise. Both regions were selected after inspection of the whole-brain VBM result, so their effect estimates serve an exploratory, descriptive purpose (Kriegeskorte et al. 2009). MRI-proximal RBDSQ severity showed no significant relationship with either regional measure, suggesting that the group-level structural contrast is not captured by a simple linear symptom–GMV association.

4.2. Relation to prior olfactory–limbic morphometry

Zhao et al. (2026) examined predefined olfactory–limbic and Papez-related regions in PPMI using matched groups, FreeSurfer/ScLimbic morphometry, and structural covariance. We asked a different anatomical question by mapping phenotype-associated GMV differences across the whole brain. The largest adjusted effect was posterior, in visual and cuneus-calcarine territory, and persisted under several scanner restrictions and nonparametric inference. Differences in anatomical coverage and analytical design account for the complementary findings. The underlying PPMI cohorts may overlap, an important consideration when interpreting their relationship.

Olfactory impairment in PD has been associated with abnormalities in the amygdala, entorhinal/parahippocampal areas, insula, orbitofrontal cortex, and related circuits (Brosse et al. 2024; Fullard et al. 2017; Saqib et al. 2025). The posterior peak in our study identifies the largest relative difference between enrollment groups in this whole-brain model. It does not define the full anatomical substrate of olfactory dysfunction.

4.3. Secondary comparisons with manifest PD

In the secondary disease-context analyses, hyposmia-only participants showed posterior GMV differences relative to manifest PD across several scanner restrictions. RBD-only versus PD findings varied more with sample composition. A left striatal PD > RBD cluster appeared in the common-support cohort but was absent under the Siemens-only restriction. Differences in clinical state, recruitment, and site representation make these cross-sectional contrasts unsuitable for ordering the groups along a disease trajectory.

Brain-first and body-first models offer one framework for interpreting prodromal heterogeneity (Berg et al. 2021; Horsager and Borghammer 2024; Orso et al. 2024). Our phenotype comparison supplies regional morphometric evidence relevant to that broader discussion, without directly testing pathological spread or conversion risk.

4.4. Sensitivity analyses, clinical timing, and interpretation

Scanner-restricted analyses retained a similar posterior localization with a stricter GM mask, common-support families, and Siemens PRISMA/SKYRA scanners. The PRISMA-only subset (N = 287) showed a comparable peak but no corrected-significant cluster. This attenuation could reflect reduced sample size, changes in participant or site composition, or a combination of these factors. Sex- and scanner-matched analysis provided a second perspective. Among 123 matched pairs, the directional H > RBD T cluster survived correction, whereas the direction-independent F cluster did not. The matched T peak was farther left and posterior to the primary peak. Different voxel-forming cutoffs contribute to the F/T discrepancy. The

matched findings therefore support a posterior directional effect in the matchable subgroup, although its extent is less stable than in the primary analysis.

The clinical measures help characterize the two recruitment groups. Hyposmia-only participants had lower screening UPSIT scores, and RBD-only participants reported more symptoms on the baseline RBDSQ. These differences align with the entry pathways. Clinical assessment dates were recorded only by month, however, and most hyposmia-only UPSIT screening records fell outside the MRI ± 90-day window. We therefore treated UPSIT as screening history; RBDSQ-BL provided the better temporally aligned symptom measure. Even with this restriction, neither posterior ROI was significantly associated with RBDSQ score. Thus, a phenotype-related morphometric difference need not vary linearly with questionnaire severity.

The whole-brain SPM and PALM findings provide complementary evidence for posterior localization. Scanner restrictions and exact matching revealed how the result changes with cohort composition, while the atlas-based analyses supplied effect estimates for the regions of interest. Clinical timing checks helped determine which symptom associations could be examined alongside MRI. Several findings were less consistent, notably the PRISMA-only, matched F, matched calcarine, and RBDSQ–ROI results. In multicenter MRI, even explicit scanner-family adjustment leaves scope for unmeasured site and protocol effects (Fortin et al. 2018; Orlhac et al. 2022).

4.5. Strengths and limitations

The study combines a post-2020 phenotype-focused PPMI sample with CAT12 and tissue-volume quality control, whole-brain inference, scanner restrictions, matched analyses, and a nonparametric assessment. Several limitations affect interpretation. The cross-sectional design provides no estimate of longitudinal tissue change or future phenoconversion. Phenotypes were assigned from PPMI enrollment flags; individual polysomnography and other diagnostic information were not independently re-adjudicated. Substantial sex, TIV, and scanner imbalances were present at baseline. Covariate adjustment and exact matching address these measured differences but leave possible confounding by site, acquisition protocol, recruitment, and other unmeasured factors.

All sensitivity analyses drew on the same PPMI participants and preprocessing pipeline, so external replication remains necessary. PALM sign-flipping also assumes approximately independent, symmetric errors after nuisance adjustment. Posterior ROI analyses were chosen after the whole-brain finding, and the atlas-integrated smoothed modulated GM measure is not equivalent to native-space anatomical volume. Questionnaire results were closely related to recruitment pathways; the clinical date field was available only to the month, and many UPSIT assessments preceded MRI by more than 90 days. The primary comparison included no healthy controls, and neither longitudinal outcomes nor an external validation cohort were examined. Confirmation in clinically verified, longitudinal samples will be needed to assess prognostic or mechanistic relevance.

5. Conclusions

Among PPMI participants enrolled from 2020 onward through hyposmia-only and RBD-only pathways, whole-brain VBM identified a posterior cortical GMV difference centered on visual and cuneus-calcarine

regions. PALM and the matched cuneus estimate were consistent with this regional finding. The matched whole-brain F test and PRISMA-only restriction did not reach corrected significance, and regional GMV was not significantly associated with MRI-proximal RBDSQ scores. Longitudinal studies in independently recruited cohorts are needed to determine its clinical significance.

Supplementary Information (Online Resource 1): Tables S1–S9 and Supplementary Figs. S1–S2 provide detailed scanner composition, whole-brain and disease-context sensitivity maps, MRI quality control, matched-pair contrasts, clinical timing, regional effect estimates, and PALM direction/spatial checks.

Declarations

Institutional Review Board Statement

PPMI was approved by the institutional review board or independent ethics committee at each participating site and was conducted in accordance with the Declaration of Helsinki and applicable regulatory requirements. The present analysis used de-identified previously collected data and involved no new participant contact.

Informed Consent Statement

Informed consent was obtained from all participants involved in the PPMI study before study procedures.

Competing Interests:

The authors declare no conflicts of interest.

Funding:

This work was supported by the Eastern Talent Plan (grant number TF2024LYLY01 to H.H.) and the Shanghai Shenkang Hospital Development Center Research Fund (grant number SHDC12026113). PPMI – a public-private partnership – is funded by the Michael J. Fox Foundation for Parkinson's Research and funding partners, including AbbVie, Alamar Biosciences, Aligning Science Across Parkinson's (ASAP), Arrowhead Pharma, Arvinas, AskBio, BIAL, BioArctic, Biohaven, BlueRock Therapeutics, Bristol Myers Squibb, Calico Labs, Capsida Biotherapeutics, Critical Path Institute, DaCapo Brainscience, Denali, Edmond J. Safra Foundation, Eli Lilly, Gain Therapeutics, GE Healthcare, Genentech, GSK, Insitro, Johnson & Johnson Innovative Medicine, Lundbeck, Merck, Neumora, Neuron23, Novartis, Olink, Regeneron, Roche, Sanofi, Tenvie, UCB, Vanqua Bio, Voyager Therapeutics, The Weston Family Foundation.

Author Contribution

L.C. and S.C. contributed equally to this work. L.C. performed the primary data analysis, interpreted the results, and drafted the manuscript. S.C. contributed to data curation, MRI quality control, CAT12/SPM

image preprocessing, statistical analysis, and critically revised the manuscript. H.H. and K.H. conceived and designed the study, supervised the project, and critically revised the manuscript. All authors have read and agreed to the published version of the manuscript.

Acknowledgments:

The authors acknowledge the participants, investigators, and study personnel of the Parkinson's Progression Markers Initiative (PPMI) for their contributions to the collection and availability of the data used in this study.

Data Availability

The data analyzed in this study were obtained on 23 June 2026 from the Parkinson's Progression Markers Initiative (PPMI) database (https://www.ppmi-info.org/access-data-specimens/download-data; RRID). PPMI data are available to researchers through the PPMI data-access process, subject to applicable access and data-use requirements. Further information about the study and data access is available at https://www.ppmi-info.org. The summary results of the present analyses are reported in the article and its Supplementary Information.

References

1. Ashburner J, Friston KJ (2000) Voxel-based morphometry - the methods. NeuroImage 11(6):805–821. https://doi.org/10.1006/nimg.2000.0582
2. Benjamini Y, Hochberg Y (1995) Controlling the false discovery rate: a practical and powerful approach to multiple testing. J R Stat Soc Ser B 57:289–300. https://doi.org/10.1111/j.2517-6161.1995.tb02031.x
3. Berg D, Postuma RB, Adler CH et al (2015) MDS research criteria for prodromal Parkinson's disease. Mov Disord 30(12):1600–1611. https://doi.org/10.1002/mds.26431
4. Berg D, Borghammer P, Fereshtehnejad SM et al (2021) Prodromal Parkinson Disease Subtypes - Key to Understanding Heterogeneity. Nat Rev Neurol 17(6):349–361. https://doi.org/10.1038/s41582-021-00486-9
5. Brosse S, Tremblay C, Merida I, Frasnelli J (2024) Specific Structural Changes in Parkinson's Disease-Related Olfactory Dysfunction Compared to Other Forms of Olfactory Dysfunction. Front Neural Circuits 18:1503841. https://doi.org/10.3389/fncir.2024.1503841
6. Campabadal A, Segura B, Junque C, Iranzo A (2021) Structural and functional magnetic resonance imaging in isolated REM sleep behavior disorder: A systematic review of studies using neuroimaging software. Sleep Med Rev 59:101495. https://doi.org/10.1016/j.smrv.2021.101495
7. Chopra A, Lang AE, Hoglinger G, Outeiro TF (2024) Towards a Biological Diagnosis of PD. Parkinsonism Relat Disord 122:106078. https://doi.org/10.1016/j.parkreldis.2024.106078
8. Di Folco C, Couronne R, Arnulf I et al (2024) Charting Disease Trajectories From Isolated REM Sleep Behavior Disorder to Parkinson's Disease. Mov Disord 39(1):64–75. https://doi.org/10.1002/mds.29662

9. Doty RL, Shaman P, Dann M (1984) Development of the University of Pennsylvania Smell Identification Test: a standardized microencapsulated test of olfactory function. Physiol Behav 32:489–502. https://doi.org/10.1016/0031-9384(84)90269-5
10. Fortin JP, Cullen N, Sheline YI et al (2018) Harmonization of Cortical Thickness Measurements Across Scanners and Sites. NeuroImage 167:104–120. https://doi.org/10.1016/j.neuroimage.2017.11.024
11. Fullard ME, Morley JF, Duda JE (2017) Olfactory Dysfunction as an Early Biomarker in Parkinson's Disease. Neurosci Bull 33(5):515–525. https://doi.org/10.1007/s12264-017-0170-x
12. Garcia-Gomar MG, Videnovic A, Singh K et al (2022) Disruption of Brainstem Structural Connectivity in REM Sleep Behavior Disorder Using 7 Tesla Magnetic Resonance Imaging. Mov Disord 37(4):847–853. https://doi.org/10.1002/mds.28895
13. Gaser C, Dahnke R, Thompson PM, Kurth F, Luders E, Alzheimer's Disease Neuroimaging Initiative (2024) CAT: a computational anatomy toolbox for the analysis of structural MRI data. GigaScience 13:giae049. https://doi.org/10.1093/gigascience/giae049
14. Goetz CG, Tilley BC, Shaftman SR et al (2008) Movement Disorder Society-sponsored revision of the Unified Parkinson's Disease Rating Scale (MDS-UPDRS): scale presentation and clinimetric testing results. Mov Disord 23(15):2129–2170. https://doi.org/10.1002/mds.22340
15. Grimaldi S, Guye M, Bianciardi M, Eusebio A (2023) Brain MRI Biomarkers in Isolated Rapid Eye Movement Sleep Behavior Disorder: Where Are We? A Systematic Review. Brain Sci 13(10):1398. https://doi.org/10.3390/brainsci13101398
16. Guo T, Guan X, Zeng Q et al (2018) Alterations of Brain Structural Network in Parkinson's Disease With and Without Rapid Eye Movement Sleep Behavior Disorder. Front Neurol 9:334. https://doi.org/10.3389/fneur.2018.00334
17. Heinzel S, Berg D, Gasser T, Chen H, Yao C, Postuma RB (2019) Update of the MDS research criteria for prodromal Parkinson's disease. Mov Disord 34(10):1464–1470. https://doi.org/10.1002/mds.27802
18. Horsager J, Borghammer P (2024) Brain-First vs. Body-First Parkinson's Disease: An Update on Recent Evidence. Parkinsonism Relat Disord 122:106101. https://doi.org/10.1016/j.parkreldis.2024.106101
19. Kriegeskorte N, Simmons WK, Bellgowan PSF, Baker CI (2009) Circular analysis in systems neuroscience: the dangers of double dipping. Nat Neurosci 12:535–540. https://doi.org/10.1038/nn.2303
20. Lyu Z, Zheng S, Zhang X et al (2021) Olfactory Impairment as an Early Marker of Parkinson's Disease in REM Sleep Behaviour Disorder: A Systematic Review and Meta-Analysis. J Neurol Neurosurg Psychiatry 92(3):271–281. https://doi.org/10.1136/jnnp-2020-325361
21. MacKinnon JG, White H (1985) Some heteroskedasticity-consistent covariance matrix estimators with improved finite sample properties. J Econom 29:305–325. https://doi.org/10.1016/0304-4076(85)90158-7
22. Marek K, Jennings D, Lasch S et al (2011) The Parkinson Progression Marker Initiative (PPMI). Prog Neurobiol 95(4):629–635. https://doi.org/10.1016/j.pneurobio.2011.09.005
23. Marek K, Chowdhury S, Siderowf A et al (2018) The Parkinson's Progression Markers Initiative (PPMI) - establishing a PD biomarker cohort. Ann Clin Transl Neurol 5(12):1460–1477.

https://doi.org/10.1002/acn3.644

24. Nasreddine ZS, Phillips NA, Bedirian V et al (2005) The Montreal Cognitive Assessment, MoCA: a brief screening tool for mild cognitive impairment. J Am Geriatr Soc 53(4):695–699. https://doi.org/10.1111/j.1532-5415.2005.53221.x
25. Oltra J, Uribe C, Segura B et al (2022) Brain Atrophy Pattern in De Novo Parkinson's Disease With Probable RBD Associated With Cognitive Impairment. NPJ Parkinsons Dis 8(1):60. https://doi.org/10.1038/s41531-022-00326-7
26. Orlhac F, Eertink JJ, Cottereau AS et al (2022) A Guide to ComBat Harmonization of Imaging Biomarkers in Multicenter Studies. J Nucl Med 63(2):172–179. https://doi.org/10.2967/jnumed.121.262464
27. Orso B, Brosse S, Frasnelli J, Arnaldi D (2024) Opportunities and Pitfalls of REM Sleep Behavior Disorder and Olfactory Dysfunction as Early Markers in Parkinson's Disease. J Parkinsons Dis 14(s2):S275–S285. https://doi.org/10.3233/JPD-230348
28. Postuma RB, Iranzo A, Hu M et al (2019) Risk and Predictors of Dementia and Parkinsonism in Idiopathic REM Sleep Behaviour Disorder: A Multicentre Study. Brain 142(3):744–759. https://doi.org/10.1093/brain/awz030
29. Saqib M, Pacheco LP, Ehrlich DJ, Horovitz SG (2025) Olfactory Network Reorganization in Parkinson's Disease. Parkinsonism Relat Disord 138:107964. https://doi.org/10.1016/j.parkreldis.2025.107964
30. Schapira AHV, Chaudhuri KR, Jenner P (2017) Non-Motor Features of Parkinson Disease. Nat Rev Neurosci 18(7):435–450. https://doi.org/10.1038/nrn.2017.62
31. Siderowf A, Heathers LEA, Fabrizio K et al (2026) Recruitment Strategies across the Spectrum of Neuronal Synuclein Disease. https://doi.org/10.1002/ana.78239. Parkinson's Progression Markers InitiativeAnn Neurol Online ahead of print
32. Smith SM, Nichols TE (2009) Threshold-free cluster enhancement: addressing problems of smoothing, threshold dependence and localisation in cluster inference. NeuroImage 44:83–98. https://doi.org/10.1016/j.neuroimage.2008.03.061
33. Stiasny-Kolster K, Mayer G, Schäfer S, Möller JC, Heinzel-Gutenbrunner M, Oertel WH (2007) The REM sleep behavior disorder screening questionnaire: a new diagnostic instrument. Mov Disord 22:2386–2393. https://doi.org/10.1002/mds.21740
34. Valli M, Uribe C, Mihaescu A, Strafella AP (2022) Neuroimaging of Rapid Eye Movement Sleep Behavior Disorder and Its Relation to Parkinson's Disease. J Neurosci Res 100(10):1815–1833. https://doi.org/10.1002/jnr.25099
35. Wang F, Zhu Z, Zhou C et al (2024) MRI brain structural and functional networks changes in Parkinson disease with REM sleep behavior disorders. Front Aging Neurosci 16:1364727. https://doi.org/10.3389/fnagi.2024.1364727
36. Winkler AM, Ridgway GR, Webster MA, Smith SM, Nichols TE (2014) Permutation inference for the general linear model. NeuroImage 92:381–397. https://doi.org/10.1016/j.neuroimage.2014.01.060
37. Wullner U, Borghammer P, Choe CU et al (2023) The Heterogeneity of Parkinson's Disease. J Neural Transm (Vienna) 130(6):827–838. https://doi.org/10.1007/s00702-023-02635-4

38. Yang C, Chang J, Liang X, Bao X, Wang R (2020) Gray Matter Alterations in Parkinson's Disease With Rapid Eye Movement Sleep Behavior Disorder: A Meta-Analysis of Voxel-Based Morphometry Studies. Front Aging Neurosci 12:213. https://doi.org/10.3389/fnagi.2020.00213
39. Zhao Y, Wang L, Suo Y, Liu M, Lin Y, Fang L, Ding Z (2026) Limbic Structural Alterations and Structural Covariance Across Prodromal Phenotypes and Early Parkinson's Disease. https://doi.org/10.1002/jmri.70544. J Magn Reson Imaging Online ahead of print

Figures

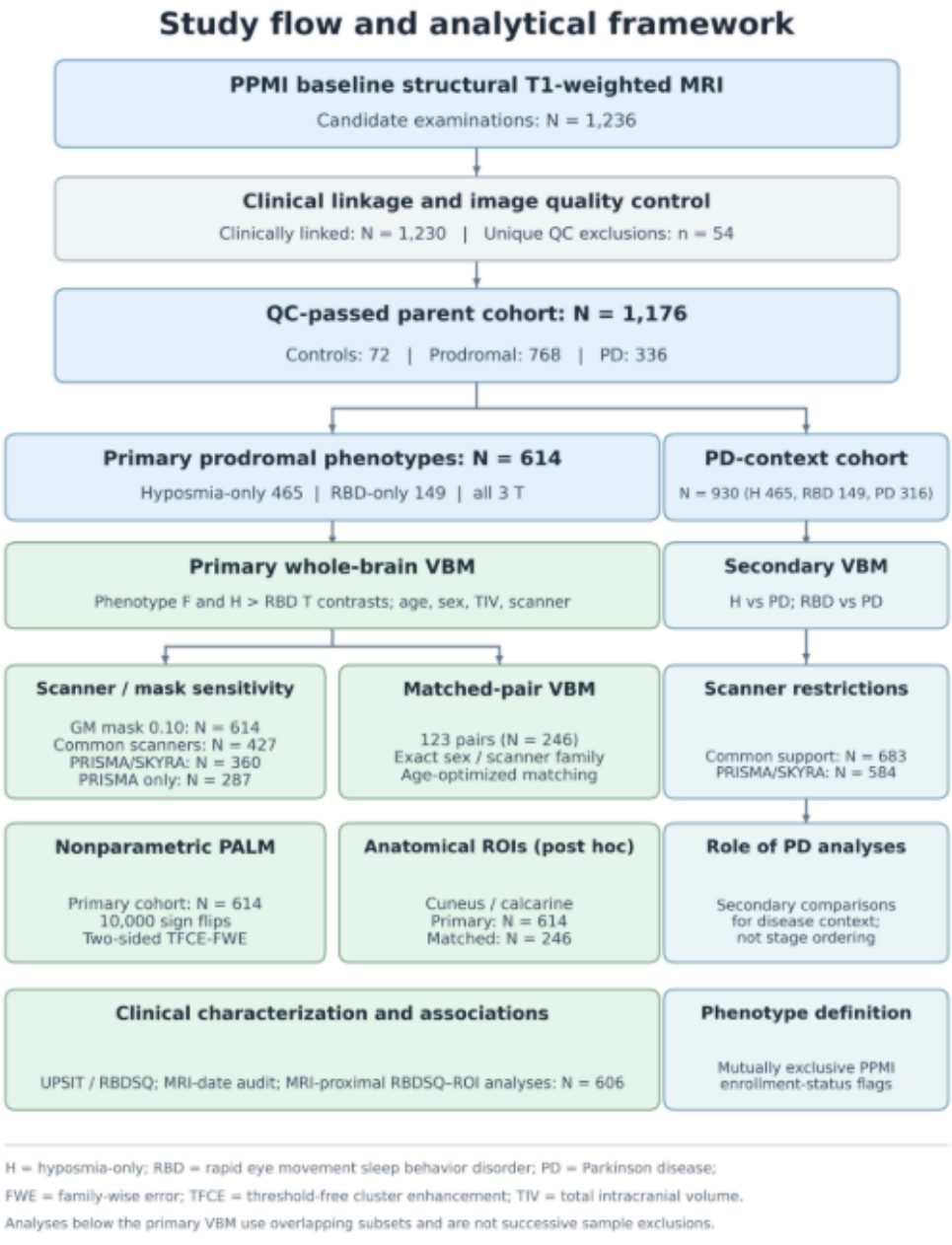


Figure 1

Study flow and analytical framework. Of 1,236 baseline MRI examinations, 1,230 were clinically linked; after 54 unique QC exclusions, 1,176 remained. The primary post-2020 cohort included 465 hyposmia-only and 149 RBD-only participants (N = 614). Additional analyses included scanner/mask restrictions, 123 matched pairs (N = 246), PALM nonparametric inference (N = 614), atlas-defined posterior ROIs, and clinical characterization (MRI-proximal RBDSQ–ROI, N = 606). Secondary disease-context comparisons included N = 930, 683, and 584

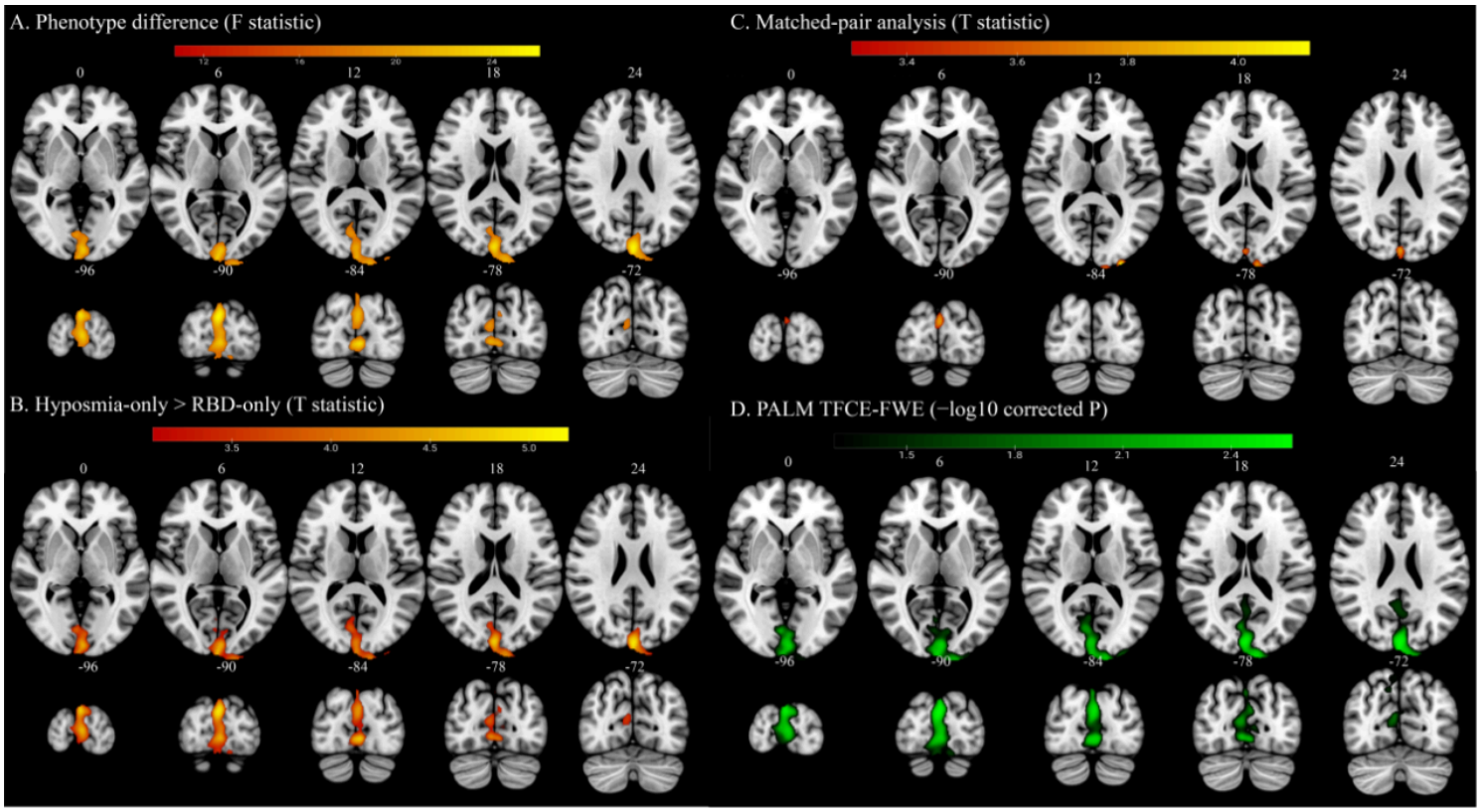


Figure 2

Convergent posterior cortical whole-brain findings in enrollment-defined Hyposmia-only and RBD-only participants. (A) Direction-independent primary phenotype F contrast (N=614). (B) Primary Hyposmia-only > RBD-only T contrast (N=614). (C) Hyposmia-only > RBD-only T contrast after exact sex- and scanner-family matching (123 pairs; N=246). Panels A–C show voxels within clusters surviving a voxel-forming threshold of P<0.001 uncorrected and cluster-level FWE P<0.05. (D) Two-sided PALM TFCE result in the original N=614 cohort (whole-brain FWE-corrected P<0.05), displayed as −log10(P_FWE) rather than a T statistic. PALM-significant voxels had positive Hyposmia-only minus RBD-only contrast values in the original SPM model. All anatomical sections are displayed in MNI space

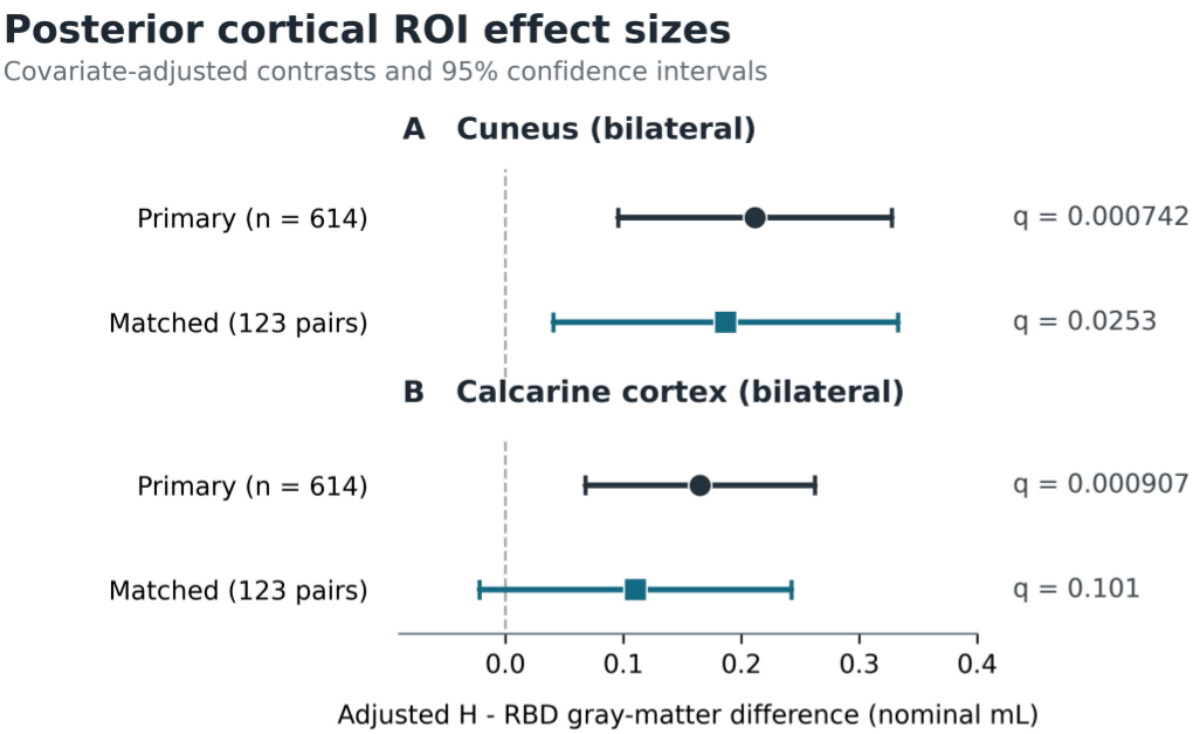


Figure 3

Exploratory posterior cortical ROI effect sizes in the primary and matched cohorts. Points represent covariate-adjusted Hyposmia-only minus RBD-only differences in bilateral cuneus and calcarine measures; horizontal lines indicate 95% confidence intervals. The primary N=614 model adjusted for age, sex, TIV, and scanner family. The matched analysis included 123 pairs (N=246) and estimated within-pair differences with age and TIV adjustment. BH-FDR q values were calculated for the two ROIs separately within each cohort. The ROIs were selected after whole-brain VBM, and matched participants were drawn from the primary cohort. Values in nominal mL represent atlas-integrated, smoothed modulated gray-matter signal, not native-space tissue volumes

Supplementary Files

This is a list of supplementary files associated with this preprint. Click to download.

- Supplementary.docx